17th World Conference on Earthquake Engineering, 17WCEE
Sendai, Japan - September 13th to 18th 2020

REGIONAL ATTENUATION MODELS IN CENTRAL AND EASTERN NORTH AMERICA USING THE NGA-EAST DATABASE

J. Bayless (1), P. Somerville (2), H.K. Thio (3), A. Skarlatoudis (4)

(1) *Engineering Seismologist, AECOM, jeff.bayless@aecom.com*
(2) *Seismologist, AECOM, paul.somerville@aecom.com*
(3) *Seismologist, AECOM, hong.kie.thio@aecom.com*
(4) *Seismologist, AECOM, andreas.skarlatoudis@aecom.com*

Abstract

The anelastic attenuation term found in Ground-Motion Prediction Equations (GMPEs) represents the distance dependence of the effect of intrinsic attenuation upon the wavefield as it propagates through the crust, and contains the frequency-dependent quality factor, $Q(f)$, which is an inverse measure of the effective anelastic attenuation. We develop improved regional estimates of $Q(f)$ in the Central and Eastern North America (CENA), building off the recent work by others including NGA-East [1], [2], and [3]. Our technique uses smoothed Fourier amplitude spectrum (FAS) data from well-recorded events in the CENA as collected and processed by NGA-East [1]. We estimate regional $Q(f)$ using (1) an assumption of average geometrical spreading applicable to the distance ranges considered, (2) a correction for the radiation pattern effect, and (3) a correction for site response based on V_{s30}. We perform independent analyses of the data adjusted for each of these effects and find that together they improve our estimates of $Q(f)$, with the site response adjustment having generally stronger influence on the attenuation modeling than the radiation pattern adjustment. Apparent $Q(f)$ estimates from multiple events are combined within each region to develop the regional models.

$Q(f)$ is usually modeled with the form $Q(f) = Q_0 f^{\eta}$, where Q_0 is the Q value at f = 1 Hz, and η is the slope parameter. Using this form, we develop models for three regions as defined by PEER [4]: The Gulf Coast, Central North America, and the Appalachian Province. There was not sufficient data to adequately constrain the model for a fourth region, the Atlantic Coastal Plain. There is general agreement that tectonically stable regions are usually described by higher $Q(f)$ and weaker frequency dependence (η), while active regions are typically characterized by lower $Q(f)$ and stronger frequency dependence (e.g. [4, 5, 2]). Our results are generally consistent with these expectations. Following a literature review and a comparison with previously published models, we conclude that our models for all three regions are valid for use.

Overall, our apparent $Q(f)$ event-based results support the Dreiling et al. (2014) [4] regionalization, as we are able to identify significantly different regional $Q(f)$ values for particular events with data recorded in multiple regions. For two events recorded in the Gulf Coast region with data both in the northernmost Mississippi Embayment (Memphis region) and to the west (Texas area), we estimate higher Q_0 in the Memphis region. We consider this region to be a candidate for potential refinement with respect to attenuation models in future investigations.

Keywords: ground motion attenuation, quality factor, CENA, stochastic method, seismic hazard

1. Introduction

In tectonically active regions of the United States, such as California, the seismicity rates are sufficient such that design ground motions can be estimated using empirical ground motion prediction equations (GMPEs, also called ground motion models, GMMs). However, for areas with low rates of seismicity, such as the Central and Eastern North America (CENA) it is challenging to develop empirical GMPEs because very few data exist, and most are for small magnitude earthquakes. Although they are infrequent, the potential for large earthquakes exists in the CENA, therefore, developing GMPEs for this region requires alternative methods beyond empirical modeling. Substantial effort has been made on this topic, including [6, 7, 8, 9, 10, 11], and most recently, the collaborative effort of the Pacific Earthquake Engineering Research Center's NGA-East [1].

When deriving GMPEs in data-poor regions, several alternatives exist, but earthquake simulations are widely used for supplementing the recorded data. Over the last several decades, the stochastic point-source method has been the commonly used simulation method for this purpose. The stochastic method is based on the pioneering work of [12, 13, 14], among others. David Boore extended it to the simulation of acceleration time series in [14] and [15]. Details in the application of this method vary, but the conventional stochastic method uses an omega-square source model [12] with a single-corner frequency and a constant stress drop [14, 16], in which the shape of the acceleration FAS spectral density Y at frequency f is given by Eq. (1).

$$Y(f) = \hat{C}\frac{f^2}{1+\left(\frac{f}{f_0}\right)^2} M_0 A(f) D(f)\, G(R) exp\left(\frac{-\pi f R}{Q(f)\beta_0}\right) \quad (1)$$

The final exponential term of Eq. (1) represents the distance dependence of the effect of intrinsic attenuation upon the wavefield as it propagates through the crust. The quality factor, $Q(f)$ is an inverse measure of effective anelastic attenuation and introduces a decay in spectral amplitudes with distance; this attenuation is frequency dependent, and thus alters spectral shape [3]. The purpose of this study is to develop improved regional estimates of $Q(f)$ in the CENA.

Taking the natural logarithm (ln) of both sides of Eq. (1) and using the product rule of logarithms yields Eq. (2). The form of this equation resembles the basic form of many GMPEs for median response spectra, $PSA_{med}(f)$, e.g. Eq. (3), where the related quantities in Eq. (2) and (3) are aligned. $Source$ is a collection of earthquake source-related terms generally described by moment magnitude (**M**) and style of faulting, $Site$ is a collection of site amplification terms (often parameterized by V_{s30} or basin depths), b is the frequency-independent geometric spreading coefficient, and $c(f)$ is the coefficient of anelastic attenuation. By Eq. 2 and 3, the relationship between $c(f)$ and $Q(f)$ is given by Eq. (4).

$$ln[Y(f)] = ln\left[\hat{C}\frac{f^2}{1+\left(\frac{f}{f_0}\right)^2} M_0\right] + ln\left[A(f)D(f)\right] + ln\left[G(R)\right] + \left(\frac{-\pi f R}{Q(f)\beta_0}\right) \quad (2)$$

$$ln[PSA_{med}(f)] = Source(f) + Site(f) + b\, ln\left[G(R)\right] + c(f)\, R \quad (3)$$

$$Q(f) = \frac{-\pi f}{c(f)\beta_0} \quad (4)$$

$Q(f)$ is believed to be attributable to intrinsic absorption, plus the frequency-dependent effects of scattering [17, 11] and is usually modeled with the form $Q(f) = Q_0 f^{\eta}$, where Q_0 is the Q value at 1 Hz, and η is the slope parameter. The geometric attenuation (b term) models the amplitude decay due to the expanding surface area of the wave front as it propagates away from the source, and generally controls the attenuation of ground motions at near source distances. At distances greater than about 100 km, the anelastic attenuation effects become dominant [11]. This is evident in Eq. 3, for which the geometric spreading attenuation scales with $\ln(R)$, and the anelastic attenuation scales with R. However, the geometric spreading and anelastic attenuation are coupled, and empirical studies have shown that the same data can be fit (for particular **M** and

distance ranges) with different trade-offs between parameters b and c. Therefore, suites of parameters developed empirically are relative to each other, and care must be taken when separately evaluating one term from one study, with another from another study. For this reason, we have chosen to fix $b = -0.5$, which corresponds to the theoretical value for surface waves in a half-space, and is a generally agreed upon value in the eastern North America at regional distances [3]. This selection is supported further in the Section 2.

1.1 Previous Work

Previous studies of regional CENA attenuation models are numerous; recent works include [2, 18, 19, 20] and NGA-East [1]. The NGA-East project was a multi-disciplinary research project managed by Christine Goulet with the objective to develop a new ground motion characterization (GMC) model for the CENA. Part of this project was to develop median GMPEs for the region, and this task included eight categories of approaches, split into ten chapters, with a different GMPE (and authors) for each chapter. Six of these chapters utilize some variation of stochastic method modeling, and therefore have either adopted or inverted models for $Q(f)$. As a starting point, NGA-East compiled attenuation (geometric spreading and anelastic attenuation) models from the literature; over 40 were identified and after review, six high quality models were selected to span the range of available models while maintaining a manageable number of models. These are summarized in Table 2.1 of [1].

The attenuation models (geometrical spreading and anelastic attenuation) used with stochastic method simulations as part of the NGA-East project are used as the basis for comparisons in Section 3. Additionally, [2] studied boundaries between major Q regions in the continental US using the Earthscope USArray data. This was accomplished using transects of observations across the transitions to look for major changes in Q. In this process, [2] determined regional estimates of apparent Q; these are also used as the basis for comparisons in Section 3. The estimates of η from [2] range from 0.5 to 0.8. These values are generally larger than those used in [1], which range from 0.3 to 0.64, with the exception of [9] which uses η = 0.84.

2. Approach

The goal of this research is to develop regional estimates of $Q(f)$, considering radiation pattern effects and site effects, which can lead to improved predictions of ground motions in the CENA. Estimating $Q(f)$ requires the knowledge of a large number of parameters including source terms, geometrical spreading, and receiver terms. A more reliable $Q(f)$ model is obtained when the size of the problem is minimized by imposing constraints on some of these parameters. Our technique includes collecting data from well-recorded events in the CENA and estimating regional $Q(f)$ using (1) an assumption of average geometrical spreading, (2) a correction for the radiation pattern effect, and (3) a correction for site response based on V_{s30}, the time-averaged shear wave velocity in the upper 30 meters of the soil column at the site. This approach is described below.

2.1 Ground Motion Data

The database used for this study is a subset of the PEER NGA-East database compiled and processed by [21]. As described in [21], this database includes events with **M** > 2.5, at distances up to 1500 km, recorded in the CENA since 1988. The final NGA-East database contains over 29,000 records from 81 earthquake events and 1379 recording stations. As is standard with all PEER NGA projects, the time series and metadata went through numerous rounds of quality assurance and review.

The ground-motion parameter used in our analysis is the smoothed EAS, as defined by and used in the PEER NGA-East GMPE (Chapter 11 of [1]). The EAS is the orientation-independent horizontal component FAS of ground acceleration. The EAS is calculated for an orthogonal pair of FAS using Eq. (5):

$$EAS(f) = \left(\frac{1}{2}[FAS_{HC1}(f)^2 + FAS_{HC2}(f)^2]\right)^{1/2} \quad (5)$$

where FAS_{HC1} and FAS_{HC1} are the FAS of the two as-recorded orthogonal horizontal components of the ground motion and f is the frequency in Hz. The FAS are processed by PEER following the procedure given by [22]. The EAS is independent of the orientation of the instrument. Using the average power of the two horizontal components leads to an amplitude spectrum that is compatible with the use of RVT to convert Fourier spectra to response spectra. The EAS is smoothed using the $\log_{10}$-scale smoothing window of [23], with smoothing parameters as described by [24].

The NGA-East project also included a working group focused on regionalization [4]. This effort divided the CENA into four regions based on the geologic and tectonic setting. These regions are shown below in Fig. 1 (reproduced from Figure 1.2 of [1]). The regions are numbered as: (1) the Gulf Coast, (2) central North America, (3) the Appalachian Province, and (4) the Atlantic Coastal Plain.

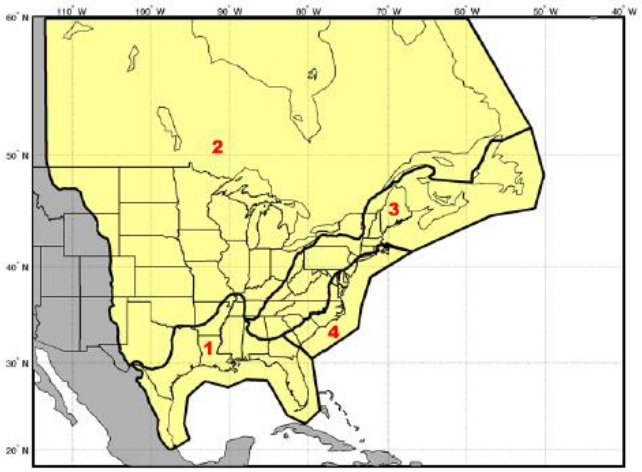

Fig. 1 – Reproduction of [1] Figure 1.2, showing the four CENA regions: (1) the Gulf Coast, (2) central North America, (3) the Appalachian Province, and (4) the Atlantic Coastal Plain.

2.2 Data Selection

The NGA-East database [21] products include a "flatfile" with recording metadata and response spectra, time series files, and FAS files. Christine Goulet provided us with a flatfile including the EAS (personal communication). In this file, the EAS has been calculated for each record in the database up to the Nyquist frequency by PEER following the [22] processing method. We determined the lowest and highest usable frequencies of each record following [25]. By limiting the usable period range, the frequency interval of the impulse response of a 5% damped oscillator will not exceed the filter values. Further, retaining this usable frequency range maintains consistency with the response spectrum models.

For each event, we select the subset of data with rupture distances between 150 and 500 km. The data at distances smaller than 150 km, for which the onset of critical reflections from the lower crust may be important [26, 27] are excluded so that the geometric spreading assumption ($b = -0.5$) is appropriate; this is also consistent with the models given in [1]. The upper limit of 500 km was selected so that the regional effects of the apparent anelastic attenuation can be observed, and also to reduce the amount of noise in the data. In addition to the quality assurance and review performed by [1], we visually checked each EAS to check for outliers, poor quality data, or errors with units. After screening for data quality, recording distance, recording coverage, and frequency limitations, we identified the 53 earthquakes as candidates for our analysis, each with at least 5 ground motion recordings. Fig. 2 shows a magnitude versus rupture distance scatterplot of this database at $f = 1$ Hz, and a map of these events along with the recording stations used in the analyses. This database encompasses over 2,000 EAS records from the 53 earthquakes. The regional $Q(f)$ estimates are derived from subsets of this database.

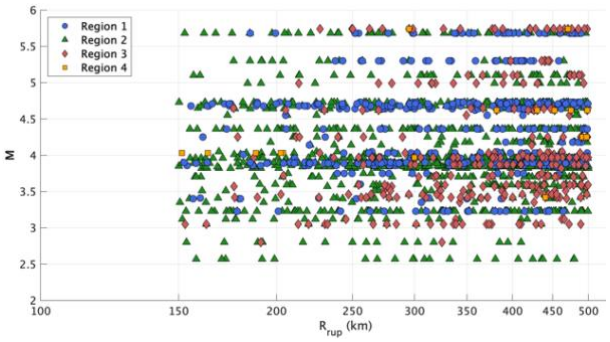

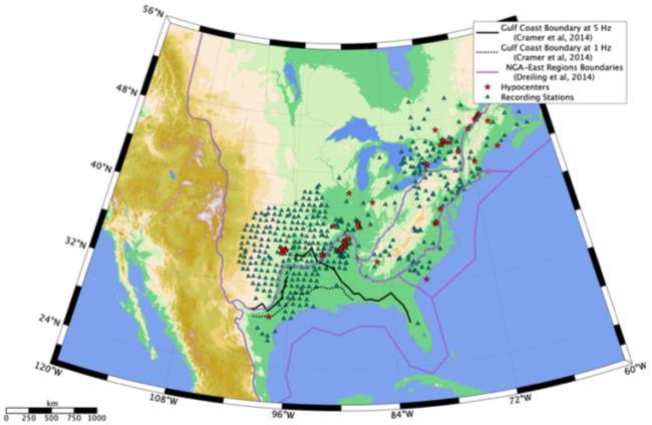

Fig. 2 – Left: Magnitude versus distance coverage of the data used in the $Q(f)$ analyses, at $f = 1$ Hz. Right: Map of epicenters for the events used (red stars), along with all recording stations (green triangles) with data available at $f = 1$ Hz. The [2, 4] region boundaries are given by the black and magenta lines, respectively.

2.3 Inversion for Q

Several studies (e.g [28, 29, 30]) have shown that radiation pattern and rupture directivity are important factors in determining the attenuation of ground motions (rate of decrease of ground motion amplitudes with distance), and that low-frequency amplitudes (in some cases up to 5 Hz) can be contaminated by radiation pattern and directivity effects. Consequently, it is preferable to take these factors into account when constructing GMPEs and $Q(f)$ models. The procedure taken to estimate the apparent $Q(f)$ for a given earthquake is as follows:

1. Gather the EAS data and metadata, filter by region as needed. The unmodified data is denoted EAS_{raw}.
2. Calculate the site response adjustment for each record, F_{Site}, as described in Section 2.3.1.
3. Calculate the radiation pattern effect adjustment for each record, F_{Rad}, as described in Section 2.3.2.
4. Adjust the EAS_{raw} for site effects (to obtain $EAS_{Site} = EAS_{raw}/F_{Site}$), for radiation pattern effects (to obtain $EAS_{Rad} = EAS_{raw}/F_{Rad}$), and for both effects to obtain $EAS_{RadSite} = EAS_{raw}/(F_{Site}F_{Rad})$.
5. Follow the [2] procedure for estimating apparent $Q(f)$. Assuming $1/\sqrt{R}$ geometrical spreading, fit the attenuation of the EAS at frequency f to Eq. (6):

$$ln[\,EAS(f)] = A(f) + b\ ln\,[R_{rup}] + c(f)R_{rup} \quad (6)$$

   where $A(f)$ is a regression constant, $b = -0.5$, R_{rup} is the closest distance to the rupture, and $c(f)$ is the apparent anelastic attenuation coefficient.
6. Estimate the apparent $Q(f)$ from $c(f)$ by the relationship given in Eq. (4). β_0 is estimated for each event by interpolating the CENA 1D crustal model from [1] Table 3.2 for the shear wave velocity at the hypocentral depth. As in [3], we impose the constraint that $c(f)$ must be negative; this corresponds to downward curvature of the attenuation of ground motions with distance. In cases where the range of the mean $c(f)$ plus and minus one standard error contained positive estimates (corresponding to flat, or upward curvature of attenuation) this frequency was excluded from subsequent analyses.

This process is repeated for each earthquake in the dataset for 10 log-spaced frequencies ranging from to 1 to 20 Hz, and for each of EAS_{raw}, EAS_{Site}, EAS_{Rad}, and $EAS_{RadSite}$. These four variations of the ground motions are analyzed to assess the effectiveness of the site and radiation pattern corrections on apparent $Q(f)$ estimates. This effectiveness is quantified through analysis of the residual standard deviations (σ_{Resid}) and the standard error of the c coefficient estimates (se_c) in Section 3.

The frequency dependence of $Q(f)$ is then fit to the form $Q(f) = Q_0 f^{\eta}$. Both this fit and the fit in Eq. (6) are performed using an iteratively re-weighted least-squares regression with Huber weighting and outlier detection [31]. In Huber weighting, observations with small residuals get a weight of one and observations with larger residual are assigned reduced weights, and the estimating equation is solved iteratively for the coefficients until convergence. The apparent $Q(f)$ estimates using this procedure are whole record estimates, which at regional distances from shallow events are dominated by the L_g phase (mixed with other phases); primarily composed of S waves trapped within the lower seismic velocities in the crust [32]. Therefore, the results presented here are compatible with other studies to determine frequency-dependent L_g attenuation in the CENA.

2.3.1 Site Response

For the site response adjustment (Inversion Step 2) we consider three existing linear models. The first is the Harmon et al. (2019) [33] linear model, which is developed specifically for smoothed FAS in the CENA. This model was developed from a parametric study of 1D ground response analyses of input rock motions propagated through soil columns representative of CENA site conditions using the software DEEPSOIL V6.1 [34]. The [33] linear FAS model is in the form of tabulated ln(amplification) as a function of V_{s30}, ranging from 90 to 3000 m/s, and f, ranging from 1 to 100 Hz. We interpolate the ln(amplification) for the V_{s30} of the site and for the frequency under consideration.

The second model considered is from [35] which as part of the NGA-East project, synthesized relevant research results to provide recommendations to the USGS for the modeling of ergodic site amplification in CENA for application in the next version of USGS maps. This panel recommended a model composed of three terms; the component used here is the linear site amplification term which describes V_{s30} scaling relative to a 760 m/s reference condition. This model is largely empirical, although it is designed for use with 5% damped pseudo-spectral acceleration instead of FAS. Because this model is based on data in the CENA it is retained as one of the options. This model is applicable for V_{s30} from 200 to 2000 m/s and $f = 0.2$ to 12.5 Hz

The third model considered is from [36], which is an empirical EAS ground motion model developed for California. One component of this ground motion model is an empirical, V_{s30} and frequency based linear site amplification term. This model is applicable for V_{s30} from 180 to 1500 m/s and $f = 0.1$ to 24 Hz. The drawback of using this model is that it is derived from data recorded in California and Nevada, which is well-known to have different geologic conditions than the CENA. However, this model is also retained because it is appropriate for correcting the smoothed EAS used in this study.

The effectiveness of these models in estimating apparent $Q(f)$ is quantified through reductions in σ_{Resid} and se_c relative to the uncorrected data, which imply that the attenuation of the data are fit better after applying the site correction. Ultimately, as discussed in Section 3, we find the best performing site response model varies between regions. In the Gulf Coast and Appalachian Province, the [35] site amplification model performs best, and in the CENA the [33] model performs best. Therefore, these two site response models are adopted for these corresponding regions for the remainder of the study. The comparison of σ_{Resid} and se_c reductions for the three site response models are given in the electronic appendix.

2.3.2 Radiation Pattern

The radiation pattern adjustment (Inversion Step 3) is based on 2-dimensional estimations obtained by averaging the 3-dimensional radiation amplitude pattern focal sphere for S waves (Equations 4.84 and 4.85 from [37]) over a narrow range of azimuths and take-off angles for a specific focal mechanism and source-receiver azimuth. The take-off angle is randomized around 30 degrees (measured from horizontal) for high frequencies, where the randomization becomes narrower as the frequencies approach 1 Hz. Following [38], this takeoff angle falls within the recommended range for regional source to site distances. Here S represents the total S motion ($= \sqrt{SH^2 + SV^2}$). For a given azimuth, the radiation coefficient is normalized by the

average over the whole focal sphere. Using this procedure, we get a dimensionless radiation amplitude pattern parameter that varies with azimuth, given the earthquake strike, rake, dip. In most cases, the radiation pattern adjustment falls within a factor of 2.

The four-lobed apparent radiation pattern is expected to be gradually distorted with increasing frequency [39]. To model the saturation of radiation pattern with increasing frequency, we follow the procedure of [40] in which, at higher frequencies, the 2D radiation pattern is washed out and becomes a circle (independent of azimuth) at 3 Hz. The σ_{Resid} and se_c reductions after accounting for site and radiation pattern effects are given in Appendix E.

2.3.3 Example Inversion

To illustrate this procedure, an example is given using data from the **M**4.7 Sparks earthquake (EQID 90) recorded in Region 1 (the Gulf Coast). Fig. 3 shows a map of the earthquake epicenter and the recording stations used in this analysis. The 2-dimensional S-wave radiation pattern at $f = 1.5$ Hz for this earthquake is shown by the dashed line. At the same frequency, this data is processed as described previously (site effects based on frequency and V_{s30}, and radiation pattern effects based on the frequency and azimuthal variation of the 2-dimensional radiation pattern). Fig. 3 shows these radiation pattern correction factors for $f = 1.5$ Hz versus azimuth (right), where the small black symbols are the 2-dimensional estimations of the total S-wave motion radiation amplitude pattern normalized by the average over the whole focal sphere, and the red circles are the recording stations. At each stage, the attenuation of the data is fit to Eq. (6), as shown in the right of Fig. 3. This procedure is repeated for multiple frequencies to estimate the frequency dependence of the apparent anelastic attenuation, c(f), and the apparent Q(f) on an event-by-event basis (e.g. Fig. 4) and these results are combined to create regional models.

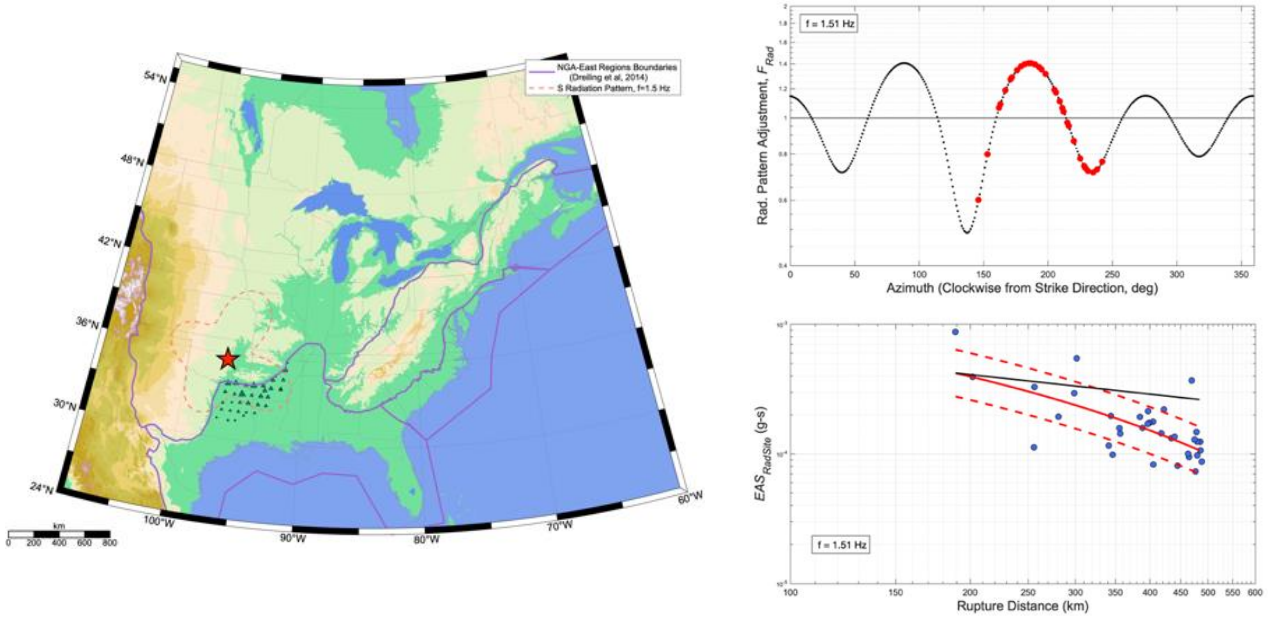

Fig. 3 – Left: A map showing the **M**4.7 Sparks earthquake epicenter (red star) and recording stations in Region 1 (green triangles) used in the inversion. The 2-dimensional S radiation pattern at $f = 1.5$ Hz is shown by the dashed line, for earthquake strike, rake, and dip of 300, 80, and -10 deg, respectively.
Top Right: Azimuthal variation of the radiation pattern adjustment, for the **M**4.7 Sparks earthquake. The small black symbols are the 2-dimensional estimations of the total S motion radiation amplitude pattern normalized by the averaged over the whole focal sphere. Red circles are the recording stations.
Bottom Right: Attenuation with distance at $f = 1.5$ Hz of the data ($EAS_{RadSite}$), along with the mean fit of Eq. 10 (red), plus and minus one standard deviation. The black curve is the geometric spreading attenuation rate ($b = -0.5$) and $Q(f)$ models the departure from this rate.

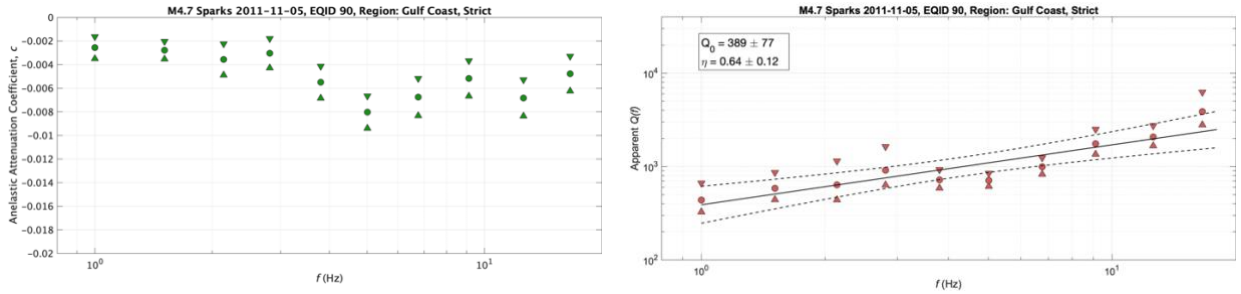

Fig. 4 – Results from the **M**4.7 Sparks earthquake (EQID 90) with data recorded in Region 1. Left: the mean apparent anelastic attenuation coefficient, c (filled circles), versus frequency, with standard error of the coefficient (triangles). Right: the apparent $Q(f)$. The mean (filled circles) and standard error (triangles) are given along with the mean fit (solid line) and 95% confidence intervals for the mean fit (dashed lines). Q_0 and η with their standard errors are given in the figure.

3. Results

Within each region, we estimate apparent $Q(f)$ independently for each event. As described previously, the inversion procedure was performed on each of EAS_{raw}, EAS_{Site}, EAS_{Rad}, and $EAS_{RadSite}$ in order to assess the effectiveness of these data corrections on modeling apparent $Q(f)$. Additionally, the procedure was repeated for each of the three alternative linear site amplification models. We selected the data correction (and model) to use based on reductions in σ_{Resid} and se_c relative to the uncorrected data. Electronic Appendix E shows these reductions, both event-based and averaged over all events within a region, for each site amplification model and NGA-East region.

Based on this assessment, we found that the radiation pattern and site adjusted ground motions ($EAS_{RadSite}$) perform best for our purposes when using the [35] site amplification model in the Gulf Coast and Appalachian regions, and using the [33] model in the Central North America region. We also found that the radiation pattern adjustment has generally weaker influence on improving the attenuation modeling than the site response adjustment. The radiation pattern adjustment also has large variability in its effectiveness, as manifested by occurrences of increases in σ_{Resid} for some events and decreases in others. This is likely an indication that our simple algorithm for the radiation pattern is too generic and could be a potential improvement for future studies.

3.1 Regional Models

To develop each regionalized model, we calculate the mean of the event-based estimates of apparent $Q(f)$ within each region. Fig. 5 shows the mean $Q(f)$ (circles) with standard deviations (triangles) for the three regions. The best fit of the mean to the form $Q_{region}(f) = Q_0 f^{\eta}$ is also shown. The regional model parameters from this fit are listed in Table 2.

Table 2 – Summary of apparent $Q_{region}(f)$ model parameters.

Region	**Region Name**	Q_0	σ_{Q_0}	η	σ_η
1	Gulf Coast	278	15	0.60	0.03
2	Central North America (CNA)	465	31	0.56	0.04
3	Appalachian Province	451	39	0.55	0.05

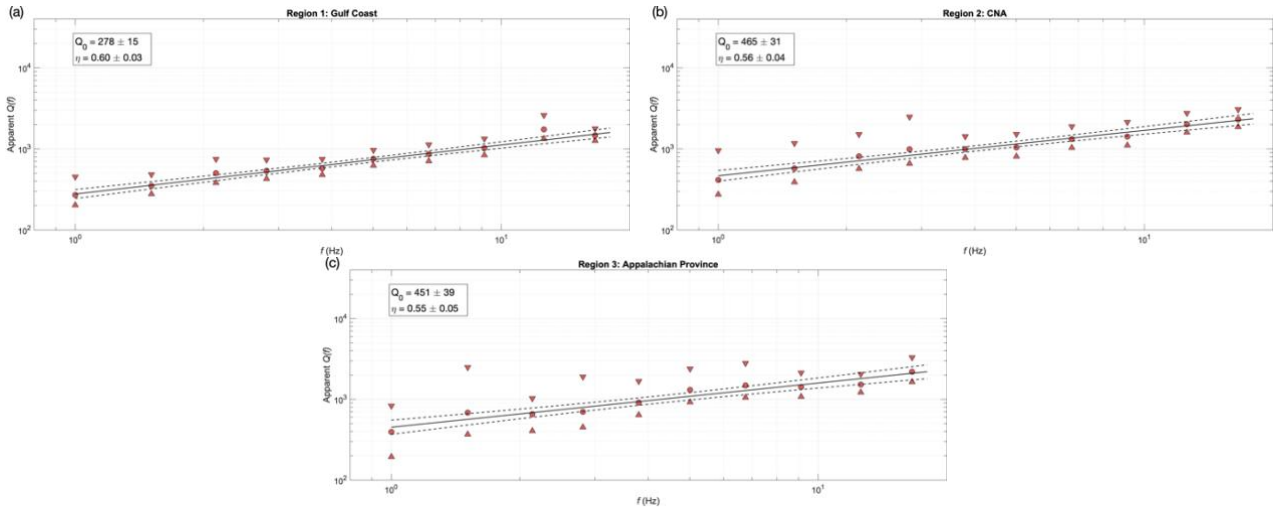

Fig. 5 – Results for (a) the Gulf Coast, (b) the CNA, and (c) the Appalachian Province showing the $\bar{Q}(f)$ (filled circles) and standard deviations (triangles) of the event-based results. The mean fit (solid line) with 95% confidence intervals (dashed lines) are shown. Values of Q_0 and η are given in each panel.

3.2 Discussion

There is general agreement that tectonically stable regions are usually described by higher $Q(f)$ and weaker frequency dependence (η), while active regions are typically characterized by lower $Q(f)$ and stronger frequency dependence [e.g. 4, 5, 2]. [5] attributed these differences to the greater amounts of interstitial crustal fluids in western North America. Further, [5] found lowest Q_0 is in the western United States, with intermediate values in the area spanning from the Colorado Plateau to the Rocky Mountains and in the southern Portion of the Atlantic Coastal Plain and the Gulf Coast, with the highest Q_0 in the Appalachians. These trends are generally consistent with our results (Table 2), although we find the differences between regions are less pronounced. Based on our analysis, Q_0 is lowest in the Gulf Coast region ($Q_0 = 278$) and larger, but similar, in the Central North America region ($Q_0 = 465$) and the Appalachian Province ($Q_0 = 451$). We also find the strongest frequency dependence in the Gulf Coast ($\eta = 0.60$), and slightly lower frequency dependence in the Appalachian Province ($\eta = 0.55$) and Central North America ($\eta = 0.56$).

The models developed here are compared with a selection of published models in Fig. 6. Two alternative Gulf Coast models, [2, 9], have stronger frequency dependence than the one developed here ($\eta = 0.60$ compared with $\eta = 0.75$ and 0.84), and the current study value of $Q_0 = 278$ lies between the Q_0 of the other two models ($Q_0 = 270$ and 351), as shown in Fig. 6a. Fig. 6b compares two models for CNA [2, 41] and six models for ENA [2, 3, 41, 42, 43, 44] with the results from this study. The CNA region used in this study (Region 2, as defined by [4]) contains the region others have described as the ENA (which generally includes northeastern United States and Southeastern Canada, but not central North America) as well as Central North America. With the exception of [43] ($Q_0 = 410$) the value of $Q_0 = 465$ from the present study is low compared with the other models, with values generally falling between 500 and 700. The slope parameter $\eta = 0.56$ from this study is consistent with the range of other models. Fig. 6c compares the [45] model for the Appalachian Province with the results from this study. Our model ($Q_0 = 451$, $\eta = 0.55$) has steeper slope and is lower at low frequencies than [45] ($Q_0 = 573.5$, $\eta = 0.465$), which results in similarity between the models at frequencies above 10 Hz.

4. Conclusions

Our technique to develop improved regional estimates of $Q(f)$ in the CENA uses smoothed *FAS* data from well-recorded events in the CENA as collected and processed by PEER NGA-East [1]. We estimate regional $Q(f)$ using an assumption of average geometrical spreading applicable to the distance ranges considered, a

correction for the radiation pattern effect, and a correction for site response based on V_{s30}. We perform independent analyses of the data adjusted each of these effects and find that together they improve our estimates of $Q(f)$, with the radiation pattern adjustment having generally weaker influence on the attenuation modeling than the site response. Apparent $Q(f)$ from multiple events are combined within each region to develop the regional models.

$Q(f)$ is usually modeled with the form $Q(f) = Q_0 f^{\eta}$, where Q_0 is the Q value at 1 Hz, and η is the slope parameter. Using this form, we develop models for three regions as defined by PEER [1]: The Gulf Coast, Central North America, and the Appalachian Province. There was not sufficient data to adequately constrain the model for a fourth region, the Atlantic Coastal Plain. The regional models are given in Table 2. Our apparent $Q(f)$ event-based results support the regionalization in [4]. A literature review and comparison with previously published models (Fig. 6) indicate that our models are suitable for estimating the $Q(f)$ for all three regions.

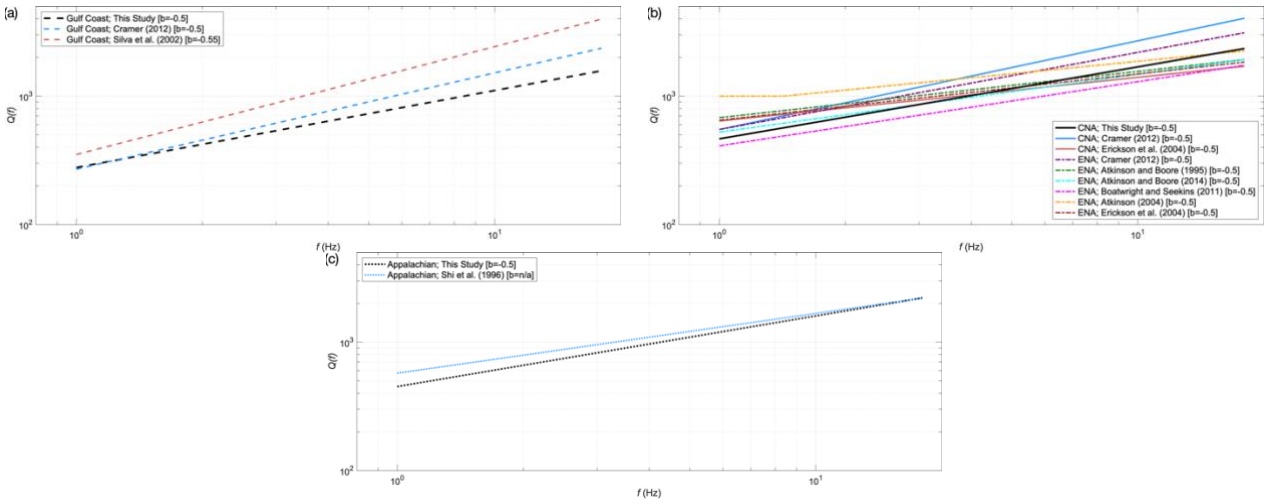

Fig. 6 – Comparison of $Q(f)$ models for (a) the Gulf Coast, (b) the CNA or ENA as noted in the legend, and (c) the Appalachian Province

5. Acknowledgements

We gratefully acknowledge the financial support for this work by the USGS under award number G17AP00034. Thanks to the Pacific Earthquake Engineering Research Center for making their ground motion databases, including those from NGA-East, publicly available. We thank Christine Goulet for her assistance with the PEER NGA-East database, and to Youssef Hashash and Okan Ilhan for providing guidance with their FAS site amplification model. All maps in this report were created using the M_Map Matlab package [46].

6. References

[1] PEER (2015) NGA-East: Median Ground-Motion Models for the Central and Eastern North America Region. April 2015.

[2] Cramer et al. (2012). Improving Regional Ground Motion Attenuation Boundaries and Models Using EarthScope USArray Data for Use in the National Seismic Hazards Mapping Project, *US Geological Survey report*, G12AP20018.

[3] Atkinson, G.M. and D. Boore (2014). The Attenuation of Fourier Amplitudes for Rock Sites in Eastern North America. *Bull. Seismol. Soc. Am.* 104, 1, 513-528.

[4] Dreiling J., Isken M.P., Mooney W.D., Chapman M.C., Godbee R.W. (2014). *NGA-East* regionalization report: comparison of four crustal regions within central and eastern north america using waveform modeling and damped

pseudo-spectral acceleration response, *PEER Report No. 2014/15*, Pacific Earthquake Engineering Research Center, University of California, Berkeley, CA.

[5] Baqer S. Mitchell B.J. (1998). Regional variation of Lg Coda Q in the continental United States and its relation to crustal structure and evolution. Pure Appl. Geophys., 153: 613−638.

[6] Boore D.M., Atkinson G.M. (1987). Stochastic prediction of ground motion and spectral response parameters at hard-rock sites in eastern North America, Bull. Seismol. Soc. Am., 77(2): 440-467.

[7] Electric Power Research Institute (1993). Guidelines for determining design basis ground motions. Volume 1. Method and guidelines for estimating earthquake ground motion in eastern North America. Report EPRI TR-102293.

[8] Toro, G. R., N. A. Abrahamson, and J. F. Schneider (1997). Model of strong ground motions from earthquakes in central and eastern North America: best estimates and uncertainties, Seism. Res. Lett. 68, 41–57.

[9] Silva, W., N. Gregor, and R. Darragh (2002). Development of regional hard rock attenuation relations for central and eastern North America, report prepared by Pacific Engineering and Analysis, El Cerrito, California.

[10] Abrahamson, N.A., and W. Silva (2001). "Empirical" attenuation relations for central and eastern U.S. hard and soft rock and deep soil site conditions, Seism. Res. Lett. 72, 282.

[11] Atkinson, G.M. (2012). Evaluation of Attenuation Models for the Northeastern United States/Southeastern Canada. Seismological Research Letters. 83, 1, 166-178. doi: 10.1785/gssrl.83.1.166

[12] Brune, J. (1970). Tectonic stress and the spectra of seismic shear-waves from earthquakes, *J. Geophys. Res.* 75, 4997–5009.

[13] Hanks TC, and McGuire RK. (1981) The character of high-frequency strong ground motion, Bull. Seismol. Soc. Am, 71, 2071–2095.

[14] Boore D.M. (1983). Stochastic simulation of high-frequency ground motions based on seismological models of the radiated spectra, Bull. Seismol. Soc. Am; 73, 1865–1894.

[15] Boore, D.M. (2003). Simulation of ground motion using the stochastic method, *Pure Appl. Geophys.* 160, 635–676.

[16] Atkinson, G. (1984). Attenuation of strong ground motion in Canada from a random vibrations approach. Bull. Seism. Soc. Am., 74, 26, 29-2653.

[17] Dainty, A. (1981). A scattering model to explain seismic Q observations in the lithosphere between 1 and 20 Hz. Geophysical Research Letters 11, 1,126–1,128.

[18] Cramer and Al-Noman (2014). Improving Regional Ground Motion Attenuation Boundaries and Models in the CEUS and Developing a Gulf Coast Empirical GMPE Using EarthScope USArray Data for Use in the National Seismic Hazards Mapping Project, *US Geological Survey 1st year report*

[19] Deshon and Bisrat (2010). Imaging Body Wave Attenuation Heterogeneity within the New Madrid Seismic Zone using Local Earthquake, *US Geological Survey report*, G10AP00013.

[20] Sandoval, E. and Yassminh, R. (2014) Seismic Attenuation and Hazard in the Central and Eastern U.S., *US Geological Survey report* , G14AP00036.

[21] Goulet, C.A., Tadahiro Kishida, Timothy D. Ancheta, Chris H. Cramer, Robert B. Darragh, Walter J. Silva, Youssef M.A. Hashash, Joseph Harmon, Jonathan P. Stewart, Katie E. Wooddell, and Robert R. Youngs. (2014). PEER NGA-East Database. PEER Report No. 2014/17. Pacific Earthquake Engineering Research Center, University of California, Berkeley, CA. October 2014.

[22] Kishida, T., O. Ktenidou, R. B. Darragh, and W. J. Silva (2016). Semi-automated procedure for windowing time series and computing Fourier amplitude spectra for the NGA-West2 database, PEER Rept. No. 2016/02, Pacific Earthquake Engineering Research Center, University of California, Berkeley, California.

[23] Konno, K., and T. Ohmachi (1998). Ground-motion characteristics estimated from spectral ratio between horizontal and vertical components of microtremor, Bull. Seismol. Soc. Am. 88, 228–241.

[24] Kottke, A., E. Rathje, D. M. Boore, E. Thompson, J. Hollenback, N. Kuehn, C. A. Goulet, N. A. Abrahamson, Y. Bozorgnia, and A. Der Kiureghian (2018). Selection of random vibration procedures for the NGA east project, PEER Rept. No. 2018/05, Pacific Earthquake Engineering Research Center, University of California, Berkeley, California.

[25] Abrahamson N.A., and Silva W.J. (1997). Empirical response spectral attenuation relations for shallow crustal earthquakes, Seismol. Res. Lett., 68(1): 94–127

[26] Burger, R.W., P.G. Somerville, J.S. Barker, R.B. Herrmann, and D.V. Helmberger (1987). The effect of crustal structure on strong ground motion attenuation relations in eastern North America, Bull. Seism. Soc. Am., 77, 420-439.

[27] Somerville, P.G., J.P. McLaren, C.K. Saikia, and D.V. Helmberger (1990). The November 25, 1988 Saguenay, Quebec earthquake: source parameters and the attenuation of strong ground motion. Bull. Seism. Soc. Am., 80, 1118-1143.

[28] Chapman, M. C., and R. W. Godbee (2012). Modeling geometrical spreading and the relative amplitudes of vertical and horizontal high-frequency ground motions in Eastern North America, *BSSA* 102, 1957–1975.

[29] Frankel, A. (2015). Decay of S-wave amplitudes with distance from earthquakes in the Charlevoix, Quebec area: Effects of radiation pattern and directivity, *Bull Seism. Soc. Am.* 105 (2a), 850-857.

[30] Graves, R. (2013), Summary of Geometrical Spreading and Q Models from Recent Events, *SMiRT-22: NGA-East Special Session*.

[31] Holland, P.W., and R.E. Welsch. (1977). "Robust Regression Using Iteratively Reweighted Least-Squares." Communications in Statistics: Theory and Methods, A6, pp. 813–827.

[32] Kennett, B. (1986). Lg waves and structural boundaries. Bulletin of the Seismological Society of America 76, 1,133–1,141.

[33] Harmon, J., Hashash, Y. M., Stewart, J. P., Rathje, E. M., Campbell, K. W., Silva, W. J., and Ilhan, O. (2019). Site amplification functions for central and eastern North America–Part II: Modular simulation-based models. Earthquake Spectra, 35(2), 815-847.

[34] Hashash, Y. M. A., Musgrove, M. I., Harmon, J. A., Groholski, D. R., Phillips, C. A., and Park, D., (2016). DEEPSOIL V6.1, User Manual, University of Illinois at Urbana-Champaign, Urbana, IL, 137 pp.

[35] Stewart, J.P., G.A. Parker, J.A. Harmon, G.M. Atkinson, D.M. Boore, R.B. Darragh, W.J. Silva, and Y.M.A. Hashash (2017). Expert Panel Recommendations for Ergodic Site Amplification in Central and Eastern North America. Report prepared for the Pacific Earthquake Engineering Research Center, University of California, Berkeley. PEER Report No. 2017/04.

[36] Bayless, J., and Abrahamson, N.A. (2019). Summary of the BA18 Ground-Motion Model for Fourier Amplitude Spectra for Crustal Earthquakes in California. *Bull. Seismol. Soc. Am.* doi: 10.1785/0120190077

[37] Aki, K.T., and P.G. Richards (1980). *Quantitative Seismology*, Freeman and Co., New York.

[38] Boore, D.M. and J. Boatwright (1984). Average Body-wave Radiation Coefficients. *Bull. Seismol. Soc. Am.* 74, 1615-1621.

[39] Takemura, S., M Kobayashi, and K. Yoshimoto (2016). Earth, Planets and Space, 68:166. DOI 10.1186/s40623-016-0544-8

[40] Pitarka, A., Somverille, P., Fukushima, Y., Uetake, T., and Irikura, K. (2000). Simulation of Near-Fault Strong-Ground Motion, *Bull. Seismol. Soc. Am.* 90 (3), 566-586.

[41] Erickson D., McNamara D.E., Benz H.M. (2004). Frequency dependent Lg Q within the continental United States, Bull. Seismol. Soc. Am., 94(5): 1630−1643.

[42] Atkinson G.M., Boore D.M. (1995). Ground motion relations for eastern North America, Bull. Seismol. Soc. Am., 85: 17–30.

[43] Boatwright J., Seekins L. (2011). Regional spectral analysis of three moderate earthquakes in northeastern North America, Bull. Seismol. Soc. Am., 101: 1769–1782.

[44] Atkinson, G.M. (2004). Empirical attenuation of ground motion spectral amplitudes in southeastern Canada and the northeastern United States, *Bull. Seismol. Soc. Am.* 94, 1079–1095.

[45] Shi J., Kim W., Richards P.G. (1996). Variability of crustal attenuation in the Northeastern United States from Lg waves, J. Geophys. Res., 101:B11 25231−25242.

[46] Pawlowicz, R., (2019). "M_Map: A mapping package for MATLAB", version 1.4k, [Computer software], available online at www.eoas.ubc.ca/~rich/map.html.

7. Appendices

Please visit the following URL to access the Appendices:
https://drive.google.com/open?id=1qzfs8DxozMRDXALnRI1Xuxvq5tliflIE

